Eur J Nucl Med Mol Imaging (2011) 38:702–710
DOI 10.1007/s00259-010-1681-0

ORIGINAL ARTICLE

A novel computer-assisted image analysis of [^{123}I]β-CIT SPECT images improves the diagnostic accuracy of parkinsonian disorders

Georg Goebel · Klaus Seppi · Eveline Donnemiller · Boris Warwitz · Gregor K. Wenning · Irene Virgolini · Werner Poewe · Christoph Scherfler

Received: 15 July 2010 / Accepted: 15 November 2010 / Published online: 21 December 2010

Abstract
Purpose The purpose of this study was to develop an observer-independent algorithm for the correct classification of dopamine transporter SPECT images as Parkinson's disease (PD), multiple system atrophy parkinson variant (MSA-P), progressive supranuclear palsy (PSP) or normal.
Methods A total of 60 subjects with clinically probable PD (n=15), MSA-P (n=15) and PSP (n=15), and 15 age-matched healthy volunteers, were studied with the dopamine transporter ligand [^{123}I]β-CIT. Parametric images of the specific-to-nondisplaceable equilibrium partition coefficient (BP_{ND}) were generated. Following a voxel-wise ANOVA, cut-off values were calculated from the voxel values of the resulting six post-hoc t-test maps. The percentages of the volume of an individual BP_{ND} image remaining below and above the cut-off values were determined. The higher percentage of image volume from all six cut-off matrices was used to classify an individual's image. For validation, the algorithm was compared to a conventional region of interest analysis.
Results The predictive diagnostic accuracy of the algorithm in the correct assignment of a [^{123}I]β-CIT SPECT image was 83.3% and increased to 93.3% on merging the MSA-P and PSP groups. In contrast the multinomial logistic regression of mean region of interest values of the caudate, putamen and midbrain revealed a diagnostic accuracy of 71.7%.
Conclusion In contrast to a rater-driven approach, this novel method was superior in classifying [^{123}I]β-CIT-SPECT images as one of four diagnostic entities. In combination with the investigator-driven visual assessment of SPECT images, this clinical decision support tool would help to improve the diagnostic yield of [^{123}I]β-CIT SPECT in patients presenting with parkinsonism at their initial visit.

Keywords [^{123}I]β-CIT SPECT · Statistical parametric mapping · Voxel-wise analysis · Deformation fields · Multiple system atrophy · Parkinson's disease · Progressive supranuclear palsy

G. Goebel (✉)
Department of Medical Statistics,
Informatics and Health Economics, Innsbruck Medical University,
Schöpfstrasse 41/2,
A-6020 Innsbruck, Austria
e-mail: georg.goebel@i-med.ac.at

K. Seppi · G. K. Wenning · W. Poewe · C. Scherfler
Department of Neurology, Innsbruck Medical University,
Innsbruck, Austria

E. Donnemiller · B. Warwitz · I. Virgolini
Department of Nuclear Medicine, Innsbruck Medical University,
Innsbruck, Austria

Introduction

The clinical assessment of an individual's cerebral MRI, PET or SPECT image is usually undertaken through the investigator's expert knowledge of the image characteristics in healthy and diseased subjects. In clinical routine, the identification of focal signal changes is frequently achieved by visual inspection or region of interest (ROI) analysis. The latter approach provides quantitative values making this technique valuable for imaging studies. ROIs can be delineated either with the help of a superimposed high-resolution structural image or by the investigator's a priori

information on the signal characteristics of the image to be analysed. Potential limitations of an investigator-driven ROI approach are related to the a priori selected size, shape and location of the brain area. For example in clinical routine the assessment of [^{123}I]-2β-carbomethoxy-3β-(4-iodophenyl) tropane ([^{123}I]β-CIT), a marker of dopamine transporter (DAT) serotonin and noradrenergic transporter availability, focuses primarily on the striatum as the brain area with the highest DAT uptake, whereas other brain regions, i.e. in the midbrain and pons, with somewhat lower but still detectable specific [^{123}I]β-CIT binding primarily to the serotonin and noradrenergic transporter might be disregarded. Additional difficulties may arise if the anatomical information provided by the functional image modality is insufficient for accurate coregistration to the structural image modality.

Advances in the evaluation of focal signal changes within the entire brain volume were achieved by transforming individual images into a standardized image space allowing voxel-by-voxel statistical comparisons between patient groups independent of an a priori hypothesis on the brain area to be analysed [1]. Following the identification of significant voxel clusters at the group level, the resulting voxel clusters are suggested for inclusion in the visual rating or ROI analysis for individual subjects. However, difficulties may be encountered if numerous voxel clusters are delivered by the between-group analysis, which, for further analysis, need to be (1) transposed to an individual subject image and (2) introduced to a decision tree handling multiple parameters for assigning a subject's individual image to a diagnosis.

Recently, voxel-based analyses of cerebral DAT distribution measured by single photon emission computed tomography (SPECT) in patient cohorts with Parkinson's disease (PD), Parkinson variant of multiple system atrophy (MSA-P), progressive supranuclear palsy (PSP) and healthy controls have identified multiple significant voxel clusters in the basal ganglia, midbrain and pons [2]. Further stepwise discriminant analysis of mean values revealed distinct ROIs with the potential to classify subjects.

To improve the accuracy of the patients' diagnosis we hypothesized in the present study that in addition to the mean value of an entire voxel cluster, the shape, size and precise location given by the voxel clusters might serve as discriminants with the potential to improve the diagnostic accuracy of quantitative image analysis.

A clinical decision support system is an information technology-based system designed to improve clinical decision making, for example to help clinicians interpret results obtained from clinical investigations, laboratory tests and medical image datasets [3, 4]. The characteristics of individual patients are matched to a computerized knowledge base, and software algorithms generate patient-specific information in the form of assessments or recommendations. Basic components of a clinical decision support system include a medical knowledge base (for example a set of rules) and an inference mechanism, which matches the rules with a patient's dataset to yield a clinical recommendation, e.g. a diagnosis or a therapeutic approach. A so-called supervised learning approach is pursued, if the knowledge base is derived from a set of training data from patients with a clinically definite diagnosis. The performance of the system can then be measured by the proportion of misclassified test cases.

We present a decision support system, referred as computer-assisted image analysis (CAIA), that was tested to assign DAT SPECT images to the diagnoses of PD, MSA-P, PSP and normal cerebral DAT distribution based on the a priori information of the disease-specific distribution of reduced DAT availability in the entire image. CAIA was tested in a proof-of-principal study design. Finally, the observer-independent CAIA algorithm was validated against a manual ROI approach entered in a multinomial regression model.

Material and methods

Subjects

Patients with MSA-P, PSP and PD (15 patients in each group) matched for age and disease duration were consecutively recruited at our movement disorder outpatient clinic and compared with a group of 15 healthy subjects matched for age. The clinical diagnosis of MSA-P, PSP and PD was made according to established criteria [5–7]. The demographic and clinical characteristics of the patients and control subjects are presented in Table 1.

A detailed clinical history and a careful neurological examination were performed. All patients were followed up clinically at least for 3 years to guarantee best possible diagnostic accuracy. In addition to [^{123}I]β-CIT SPECT, cerebral MRI was performed in order to exclude those with severe white matter, vascular or space-occupying lesions within the cerebrum. Motor disability related to parkinsonism was assessed in all patients following 12 h off drugs using part III of the Unified Parkinson's Disease Rating Scale [8]. This study was approved by the Ethics Committee of Innsbruck Medical University. Consent was obtained from all subjects in accordance with the requirements of the Declaration of Helsinki.

Table 1 Demographic and clinical characteristics of patients with PD, MSA-P and PSP and control subjects. The data presented are means±SD, 15 subjects per group

Group	Age (years)	Sex (M/F)	Disease duration (years)	Motor score (unified Parkinson's disease rating scale)
Control	64±8.7	9/6	–	–
PD	61.3±6.8	10/5	1.7±0.8	21.5±7.2
MSA-P	61.8±9.3	8/7	2±0.8	38.9±10.7*
PSP	65.5±7.2	7/8	2±0.9	35.1±6.7*

Intergroup differences were calculated by one-way analysis of variance with post hoc least statistical significance correction.
*$p < 0.001$ vs. PD patients.

Radiopharmaceutical preparation

[^{123}I]β-CIT was obtained from the Austrian Research Center, Seibersdorf. Radiolabelling, radiochemical purity, radiopharmaceutical safety and dosimetry of the tracers have been reported elsewhere [9].

Scanning protocol

After blockade of thyroid uptake with 600 mg sodium perchlorate orally 30 min before tracer administration, patients and controls received a bolus dose of 148–185 MBq [^{123}I]β-CIT intravenously. The patient's head was positioned in a head holder by means of a crossed laser beam system. Data acquisition started 18 h after tracer administration and lasted for 42 min and 40 s [10]. All scans were performed with a dual-detector ADAC VertexPlus scintillation camera (EPIC detector system, VXHR collimator) with a spatial resolution of 12 mm full-width at half-maximum in the transaxial plane. Camera heads were equipped with low-energy collimators. For each scan, a total of 64 projections (80 s per frame) were collected in step-and-shoot mode. The image data were reconstructed by standard filtered back-projection using a gaussian weighted ramp filter (cut-off frequency 0.38, order 20) and attenuation was corrected using Chang's first-order method (attenuation coefficient μ=0.12 cm^{-1}).

Data analysis

The reversible binding characteristics and the stability of regional [^{123}I]β-CIT uptake 18 h after administration permitted estimation of the binding potential which was calculated according to the equilibrium model introduced by Laruelle et al. [10]. [^{123}I]β-CIT binding potential (specific-to-nondisplaceable equilibrium partition coefficient, BP_{ND}) was determined as the ratio of specifically bound radioligand to nondisplaceable ligand in the occipital cortex. Under equilibrium conditions, BP_{ND} has been shown to be proportional to B_{max}, the maximum receptor concentration, and can be computed for every voxel from the equation [11]:

BP_{ND} = [(counts per minute/voxel)V_T − (counts per minute/voxel)V_{ND}]/(counts per minute/voxel)V_{ND}, where V_{ND} is the distribution volume of the nondisplaceable compartment relative to the total concentration of ligand in plasma and V_T is the distribution volume of total ligand uptake in tissue relative to the total concentration of ligand in plasma [12].

Calculation of ROIs

For validation of the classification algorithm by multinomial regression analysis, five ROIs were outlined by inspection of transversal [^{123}I]β-CIT SPECT images using the software package MRICro 1.37 [13]. The images included the head of the caudate nucleus (circle, diameter 10 mm), the putamen (two circles, diameter 10 mm each) and the midbrain (circle, diameter 16 mm). ROIs were positioned on the anatomically more detailed raw data [^{123}I]β-CIT image in native space and subsequently transferred to the parametric [^{123}I]β-CIT BP_{ND}image of identical image space for calculation of mean values. Right and left caudate and putaminal [^{123}I]β-CIT uptake was averaged for each subject to allow statistical analysis.

Statistical parametric mapping analysis

Image transformation, computation of BP_{ND} and statistical analysis were conducted using SPM5 [1] implemented in Matlab 7.01 (Mathworks, Sherborn, MA). As there is insufficient anatomical detail in parametric images of [^{123}I]β-CIT BP_{ND}, an indirect approach introduced by Rakshi et al. for [^{18}F]fluorodopa PET images was employed to achieve accurate spatial normalization [14]. Since a [^{123}I]β-CIT raw data image and a summed [^{18}F] fluorodopa PET image provide similar anatomical information, the raw data [^{123}I]β-CIT image of each control subject was normalized onto the in-house made [^{123}I]β-CIT

template image in MNI (Montreal Neurological Institute) space, and the resulting transformation parameters were then applied to the corresponding subject's parametric BP_{ND} image [2]. To calculate V_{ND}, a mask of the occipital cortex as defined by the Brodmann brain template provided with the software package MRIcro 1.37 [13] was extracted and transformed onto the [^{123}I]β-CIT image by inverting the deformation fields obtained when normalizing images onto the [^{123}I]β-CIT template image [15]. Consequently, for each individual SPECT acquisition a parametric BP_{ND} image was calculated. Parametric [^{123}I]β-CIT images were normalized into MNI space by applying the deformation maps previously obtained.

Each group of subjects was randomly divided into a training set comprising 12 subjects and a test set comprising 3 subjects [16]. The training sets were subjected to one-way analysis of variance followed by the application of *t*-contrasts in order to detect significant signal alterations when comparing the PD, MSA-P, PSP and control groups. SPM maps surviving a threshold of $p < 0.001$ at the cluster level were further corrected for multiple comparisons according to the random field theory [17]. Since DAT densities are known to be low in the occipital lobe and the cerebellum, a brain mask for those areas was created in order to minimize voxels of no interest for multiple comparison corrections. A total of 61,744 voxels were analysed.

Subjects assigned to the test sets remained for validating the classification procedure described below (Fig. 4). Data were processed on a Windows XP workstation (Pentium 4, Sony PCV-RS404).

Classification of patients according to computer-assisted image analysis

Voxel clusters of significant differences between groups obtained by *t*-contrasts from the analysis of variance were extracted and cut-off values were calculated for each single voxel as follows: (1) the means of the BP_{ND} and its confidence intervals (95% CI) for each group were calculated for each voxel and (2) the cut-off value for each voxel was determined by averaging between the lower boundary of the CI of one group and the upper boundary of the other group, leaving six distinct matrices of cut-off values between the four groups (Figs. 1 and 2). All cut-off matrices were transposed to the image space by inverting the deformation fields [15]. For each subject from the test set the image volume above and below each cut-off matrix was calculated and expressed as percentage volume in relation to the entire cut-off matrix (PVCM). The classification of a subject's [^{123}I]β-CIT image to a diagnosis was performed in two steps (Fig. 2). First, when comparing a subject's parametric BP_{ND} image with the cut-off matrices, six assignments to one of four possible diagnoses were obtained by classifying the individual's [^{123}I]β-CIT SPECT parametric image according to the higher PVCM value. Second, the classification to a diagnosis was made if a diagnostic entity was hit three times according to the algorithm illustrated in Fig. 3.

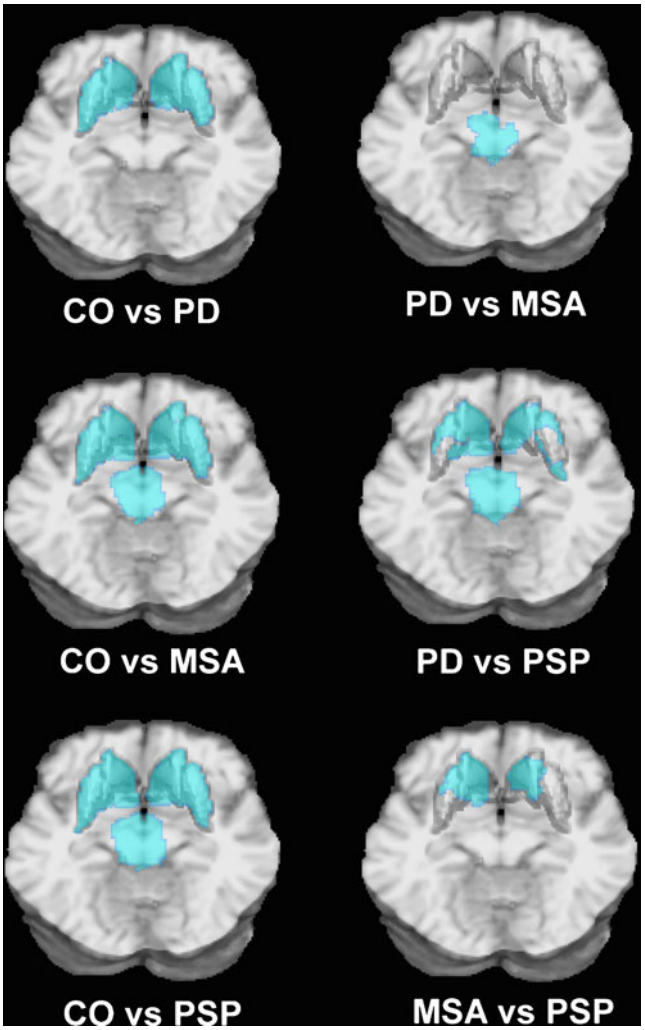

Fig. 1 Six voxel clusters representing significant between-group [^{123}I]β-CIT BP_{ND} *t*-contrasts (*blue*) following analysis of variance were extracted from the SPM analysis and rendered on to stereotactically normalized 3-D MRI scans

The entire procedure, referred to as one "run", comprising the randomization of patients to the training and test set, the SPM analysis and the classification algorithm, was performed using a random five-fold cross-validation procedure [16] (Fig. 4). Each patient was selected at least once in the training population. The classification accuracy was calculated as average percentage of the overall numbers of classified cases related to all cases in the test sets.

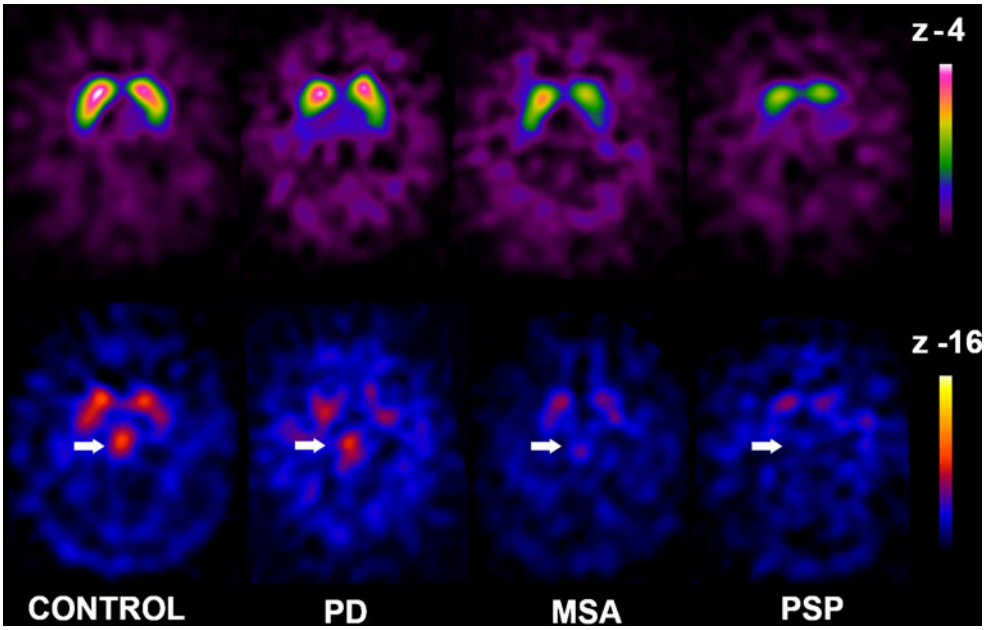

Fig. 2 Individual dopamine transporter SPECT images normalized to MNI space showing different [^{123}I]β-CIT uptake patterns in the striatum (*upper row*) and the brainstem (*lower row*, *arrows*) of a healthy control subject and patients with Parkinson's disease (*PD*), multiple system atrophy (*MSA*) and progressive supranuclear palsy (*PSP*). Numbers correspond to the *z* coordinate in MNI space

Reference method

CAIA was validated by the manual ROI approach outlined above. Mean ROI values of the caudate, putamen and midbrain were entered into a multinomial regression model with a ridge estimator [18, 19] as reference method for the assignment of a [^{123}I]β-CIT image to one of four diagnostic entities. Ridge regression models are often successfully used in situations where correlations between the predictors appear. For our experiments we used the implementation provided by the Waikato Environment for Knowledge Analysis package 3.4.13 [20].

```
Inputs:  percentage volumes of the entire cut-off matrix (PVCM)
Outputs:         assigned diagnosis

IF
      co > msa  AND co > psp AND co > ipd
      THEN group := co END
      {patient is assigned to control group}
ELSEIF
      ipd > msa  AND ipd > psp AND ipd > co
      THEN group := ipd END
      {patient is assigned to PD group}
ELSEIF
      msa > ipd  AND msa > psp AND msa > co
      THEN group := msa END
      {patient is assigned to MSA-P group}
ELSEIF
      psp > msa  AND psp > ipd AND psp > co
      THEN group := psp END
      {patient is assigned to PSP group}

ELSE
      group:= no decision possible
END.
```

Fig. 3 Computer-assisted image analysis. Classification pseudocode for the assignment of an individual's dopamine transporter SPECT image to the diagnoses: normal (control group, *co*), Parkinson's disease (*pd*), multiple system atrophy (*msa*) or progressive supranuclear palsy (*psp*)

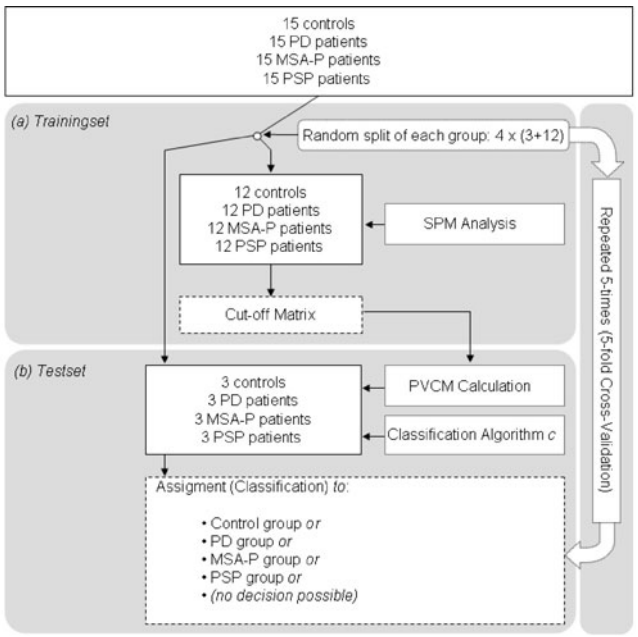

Fig. 4 Diagnosis assignment procedure based on (*a*) 48 randomly drawn individuals (12 from each group) followed by (*b*) the assignment of the 12 remaining test patients (three from each group) to one of the four diagnosis classes. The procedure was repeated five times and the assignment of the test patients to a diagnostic entity was averaged over the five runs

Results

Patients

Patient groups and control subjects were matched for age. Maximum disease duration did not exceed 3.5 years and was not significantly different between PSP, MSA-P and PD patients. MSA-P and PSP patients showed significantly greater motor disability than PD patients as assessed by the unified Parkinson's disease rating scale ($p < 0.001$; Table 1).

ROI analysis of [^{123}I]β-CIT SPECT

Regional mean [^{123}I]β-CIT BP_{ND} values of the study groups and the intergroup statistics are detailed in Table 2. One-way analysis of variance showed significant decreases in the caudate and putamen [^{123}I]β-CIT uptake in MSA-P ($p < 0.001$), PSP ($p < 0.001$) and IPD ($p < 0.001$) patients versus normal control subjects. There was no significant difference in striatal [^{123}I]β-CIT uptake between MSA-P, PSP and IPD patients. The midbrain ^{123}I]β-CIT BP_{ND} values were significantly lower in patients with MSA-P and PSP than in those with PD and the control subjects, while there was no significant difference in midbrain ^{123}I]β-CIT BP_{ND} between the PSP and MSA-P patients.

[^{123}I]β-CIT SPECT SPM analysis of variance

SPM of parametric [^{123}I]β-CIT BP_{ND} images revealed significant decreases in BP_{ND} values in the striatum of patients compared with controls (runs 1–5; $p < 0.001$, corrected). Additional significant relative decreases were seen in the ventral and dorsal midbrain and the pons in MSA-P and PSP patients (areas of the red nucleus, substantia nigra and raphe nuclei) compared with PD patients (runs 1–5; $p < 0.001$, corrected). A significant relative reduction of [^{123}I]β-CIT uptake was further evident in the caudate of patients with PSP when compared with MSA-P patients (runs 1, 2 and 4, $p < 0.001$, corrected; runs 3 and 5, $p < 0.01$, corrected). No significant increases in [^{123}I]β-CIT BP_{ND} values were detected in MSA-P versus PSP patients, in PD versus MSA-P and PSP patients or in the control subjects versus the PD, MSA-P and PSP patients.

Table 2 Mean regional putamen and caudate [^{123}I]β-CIT BP_{NP} in MSA-P, PSP and IPD patients and control subjects. Values are means ±SD

Group	Caudate	Putamen	Midbrain
Control	10.4±1.5****	10.5±1.4***·****	2.4±0.6
PD	6.4±1.5***	6.2±1.6***	2.6±0.5
MSA-P	5.6±2.0***·****	5.8±2.3***	1.6±0.7*·****
PSP	3.4±2.0***·****	3.7±1.9***·****	1.4±0.9***·****

Differences between groups were tested by one-way analysis of variance with post hoc least statistical significance correction.

*$p < 0.05$, **$p < 0.01$, ***$p < 0.001$, vs. controls.

****$p < 0.01$, vs. PD patients.

Discrimination among control subjects, and PD, MSA-P and PSP patients by computer-assisted image analysis

Overall, in five runs comprising a total of 60 independently tested subjects, 50 subjects were correctly classified (diagnostic accuracy 83.3 %; Table 3). In the PD and MSA-P groups one patient each was randomly chosen twice to enter the test sets, but in different RUNs. In the control and in the PSP group, one patient each was randomly drawn three times, again in different runs. Two control subjects, two PSP patients, one PD patient and one MSA-P patient were not selected for one of the test sets. Overall, CAIA correctly classified every control subject of the test sets and did not wrongly assign any of the patients to the entity "normal cerebral DAT distribution". Of the 15 PD patients, 13 were classified correctly; one PD patient was falsely classified to the MSA-P group and one to the PSP group. Of the PSP patients, 13 were correctly identified; one PSP patients was incorrectly assigned to the MSA-P group and one to the PD group. In none of the patients was the result "no decision possible" (ELSE condition in Fig. 3). The classification error increased in the MSA-P group: nine test cases were discriminated correctly, but five were wrongly assigned to the PSP group and one to the PD group. Since the disease course and therapeutic options in PSP and MSA-P are similar, these groups were merged to a single cohort called "atypical parkinsonian disorders" (APD). Applying the classification procedure to patients with PD or APD and control subjects, the diagnostic accuracy increased to 93.3%.

Discrimination among control subjects, and PD, MSA-P and PSP patients by multinomial logistic regression

Multinomial logistic regression of mean ROI values of the caudate, putamen and midbrain revealed a diagnostic accuracy of 71.7% (Table 4). Of the 15 control subjects, 1 was incorrectly assigned to the PD group. Of the 15 PD patients, 10 were correctly assigned and 5 were incorrectly assigned, 2 to the control group, 2 to the MSA-P group and 1 to the PSP group. Of the 15 MSA-P patients, 9 were correctly assigned and 6 were incorrectly assigned, 3 to the PD group and 3 to the PSP group. Of the 15 PSP patients, 10 were correctly assigned and five were incorrectly assigned, 1 to the PD group and 4 to the MSA-P group.

Table 3 Diagnostic classification matrix according to computer-assisted image analysis of cerebral [^{123}I]β-CIT distribution

Clinical classification	Predicted group by cerebral [^{123}I]β-CIT distribution			
	Controls	PD	MSA-P	PSP
Controls	**15 (100%)**	0	0	0
PD	0	**13 (86.7%)**	1 (6.7%)	1 (6.7%)
MSA-P	0	1 (6.7%)	**9 (60%)**	5 (33.3%)
PSP	0	1 (6.7%)	1 (6.7%)	**13 (86.7%)**

Bold indicates correct diagnosis.

After merging the MSA-P group and the PSP group (APD group) the diagnostic accuracy increased to 88.3%.

Discussion

For the first time a fully automated and observer-independent algorithm classifying individual images to one of four diagnostic entities has been described and evaluated using a [^{123}I]β-CIT SPECT brain image dataset including patients with PD, MSA-P or PSP and control subjects with a normal cerebral DAT status (Fig. 2). Voxel by voxel [^{123}I]β-CIT SPECT between-group analysis revealed alterations in monoaminergic transporter availability in multiple brain areas including the caudate, putamen, and midbrain as reported previously [2, 21]. When using these regions as discriminants for classifying an individual image, difficulties have been encountered as voxel clusters of significant signal changes between patient groups partly overlap. In a first approach, discrimination among subjects has been achieved by extracting mean voxel cluster values and subjecting them to a step-wise discriminant analysis [2, 21]. However, focusing the discrimination analysis on the mean voxel cluster values alone limits the accuracy of the classification procedure, as it does not account for either the size of voxel clusters or the distinct variation of values within the cluster.

In contrast, CAIA considers both focal differences in [^{123}I]β-CIT signal changes and the morphometry of signal distribution. In a first step, signal changes have been identified by performing a voxel-wise analysis of variance with post hoc *t*-tests of individual parametric [^{123}I]β-CIT images using SPM. Instead of extracting the mean BP_{ND} values of every voxel cluster, cut-off values for each single voxel within the voxel clusters were calculated and transposed onto the individual parametric image. Ideally cut-off values should be spatially independent to account for differences within a single voxel cluster. Voxels within a SPECT image, however, are highly correlated due to the low spatial resolution of the scanner and the processing of images including reslicing and smoothing. The random field theory implemented into SPM accounts for spatially correlated voxels and yields significantly different voxel clusters, which are assumed to be independent. For further image analysis, however, rather than calculating the cut-off value of each independent voxel cluster, the cut-off value of each voxel within these clusters were calculated for two reasons: (1) the determination of the cut-off values of each independent voxel cluster results in numerous independent parameters that would require a large number of subjects for classification; (2) the cut-off values of each voxel within a voxel cluster, although spatially correlated, provides information on the anatomical size and shape and this information would be lost if only independent clusters were considered.

In order to account for the attributes "size" of significant voxel clusters and "small number of independent variables", the parameter "percentage volume of the entire cut-off matrix" (PVCM) was calculated. The PVCM is an index that represents the proportion of voxels of a parametric BP_{ND} image that belong to one of two diagnostic entities. Since the PVCM is computed from multiple voxels from the parametric BP_{ND} image by inverting the deformation fields, the morphometry of the voxel clusters localized on the individual BP_{ND} image is taken into account as well.

The discrimination procedure resulted in high classification accuracy which could not have been predicted by visual inspection or ROI analysis of [^{123}I]β-CIT SPECT

Table 4 Diagnostic classification matrix according to multinomial logistic regression analysis of the ROI analysis of [^{123}I]β-CIT binding in the caudate, putamen and midbrain

Clinical classification	Predicted group by cerebral [^{123}I]β-CIT distribution			
	Controls	PD	MSA-P	PSP
Controls	**14 (93.3%)**	1 (6.7%)	0	0
PD	2 (13.3%)	**10 (66.7%)**	2 (13.3%)	1 (6.7%)
MSA-P	0	3 (20%)	**9 (60%)**	3 (20%)
PSP	0	1 (6.7%)	4 (26.7%)	**10 (66.7%)**

Bold indicates correct diagnosis.

images. The routine assessment of a [^{123}I]β-CIT SPECT image focuses primarily on the striatum as the brain area with the highest DAT uptake, whereas regions of the brain with somewhat lower but still detectable [^{123}I]β-CIT uptake lack anatomical information forcing the investigator to generate an a priori assumption on the morphometry of the region to be delineated. Even if the midbrain was included in the manual ROI analysis, the diagnostic accuracy revealed by the multinomial regression analysis was inferior to CAIA, supporting the use of an observer-independent voxel-driven approach. No a priori hypothesis regarding the localization of SPECT signal is required by CAIA, assuming that the spatial normalization and inversion of deformation fields is precise. The accuracy of the placement of voxel clusters was evaluated by comparing the individual SPECT images with duplicate images generated by spatial normalization onto the [^{123}I]β-CIT template image and inverting the obtained deformation fields of the normalized SPECT image (results not reported here).

Neither the ROI analysis nor CAIA revealed any significant differences in [^{123}I]β-CIT signal distribution within the striatum of the PD and MSA patients. Lower caudate DAT and [^{18}F]dopa signals have been reported in MSA patients than in PD patients [22–24]. Our voxel-based approach did not reproduce this finding, which might be attributable to the variable variance of the ROI data as a result of (1) not standardizing the positioning of the ROIs without guidance of structural MRI scans, (2) different scanner resolutions, and (3) the inclusion of patients in early disease stages without reports on diagnostic re-evaluation at follow-up visits. Predictive accuracy was high when discriminating between healthy subjects and patient groups. Good discrimination was also observed between patients with PD and those with APD, which is due to the reduced monoaminergic transporter availability in the brainstem of MSA-P and PSP patients. This finding is consistent with neuropathological observations showing distinct neuronal loss in brainstem areas containing DAT-, SERT- or NAT-bearing neurons such as the substantia nigra, the locus coeruleus and the raphe nuclei in MSA-P and PSP [25–30]. A higher error was evident in discriminating between PSP and MSA-P patients as a result of overlapping PVCMs in the brainstem and putamen which were due to a lower level of significant differences in the BP_{ND} signal.

Regarding practicability and applicability, several issues need to be considered. First, in the absence of post-mortem verification, misdiagnosis cannot be entirely excluded. However, clinical diagnoses were based on stringent clinical criteria including follow-up visits over a period of at least 3 years after the imaging study without a change in diagnosis [31, 32]. At the expense of tight inclusion criteria, the application of CAIA so far is constrained to patients between 57 and 71 years of age, with a maximum disease duration of 3.5 years, and no history of the use of selective serotonin reuptake inhibitors. The algorithm was validated in a proof-of-principle design in clinically definite cases. To assess the predictive accuracy in routine clinical practice, patients with a clinically uncertain diagnosis with subtle or incomplete features of an idiopathic parkinsonian syndrome need to be tested and validated against the clinical gold-standard of a 1-year follow-up investigation by a movement disorder specialist. Second, in order to minimize variability between scans, the [^{123}I]β-CIT images for the training and test datasets have to be acquired on the same scanner, restricting the application of CAIA to a particular tomograph, unless phantom studies become available evaluating inter-scanner calibration factors. Third, the low spatial resolution of a conventional dual headed SPECT camera together with partial volume effects lead both to spill-over effects from areas with higher [^{123}I]β-CIT uptake into adjacent brain areas and to underestimation of the radioactivity concentration in small objects [33–35]. Both effects limit the application of CAIA to anatomical structures smaller than twice the full-width at half-maximum resolution of the scanner.

Conclusion

CAIA provides an investigator-independent procedure for the classification of quantitative brain images and was shown to extend the application of [^{123}I]β-CIT SPECT as a powerful and widely available tool to improve the diagnostic yield in patients presenting with parkinsonism at their initial visit. In the future, it will be important to see if the diagnostic accuracy of CAIA holds for patients presenting with inconclusive clinical signs. Also it remains to be confirmed if the method can be applied to other parametric imaging datasets from PET, SPECT and MRI. CAIA may also be used in situations with more than four categories, provided that a-priori information of signal differences can be identified at the group level. Any enlargement of classification ability, however, would be associated with a substantial increase in the size of the training set required to build the model.

Acknowledgments The study was supported by the Austrian Federal Ministry of Science and Transport (GZ 70038/2 PR 4/98).

Conflicts of interest None.

References

1. Friston KJ, Ashburner J, Frith CD, Poline JB, Heather JD, Frackowiak RS. Spatial registration and normalization of images. Hum Brain Mapp. 1995;3:165–89.
2. Scherfler C, Seppi K, Donnemiller E, Goebel G, Brenneis C, Virgolini I, et al. Voxel-wise analysis of [123I]β-CIT SPECT

differentiates the Parkinson variant of multiple system atrophy from idiopathic Parkinson's disease. Brain. 2005;128:1605–12.
3. Haynes RB, Wilczynski NL. Effects of computerized clinical decision support systems on practitioner performance and patient outcomes: methods of a decision-maker-researcher partnership systematic review. Implement Sci. 2010;5:12.
4. Garg AX, Adhikari NK, McDonald H, Rosas-Arellano MP, Devereaux PJ, Beyene J, et al. Effects of computerized clinical decision support systems on practitioner performance and patient outcomes: a systematic review. JAMA. 2005;293(10):1223–38.
5. Gilman S, Low P, Quinn N, Albanese A, Ben-Shlomo Y, Fowler C, et al. Consensus statement on the diagnosis of multiple system atrophy. American Autonomic Society and American Academy of Neurology. Clin Auton Res. 1998;8:359–62.
6. Litvan I, Agid Y, Calne D, Campbell G, Dubois B, Duvoisin RC, et al. Clinical research criteria for the diagnosis of progressive supranuclear palsy (Steele-Richardson-Olszewski syndrome): report of the NINDS-SPSP international workshop. Neurology. 1996;47:1–9.
7. Hughes AJ, Daniel SE, Kilford L, Lees AJ. Accuracy of clinical diagnosis of idiopathic Parkinson's disease: a clinicopathological study of 100 cases. J Neurol Neurosurg Psychiatry. 1992;55:181–4.
8. Fahn S, Elton RL. Members of the Unified Parkinson's Disease Rating Scale Development Committee: Unified Parkinson's disease rating scale. In: Fahn S, Marsden CD, Calne DB, Goldstein M, editors. Recent developments in Parkinson's disease, vol 2. Florham Park, NJ: Macmillan Healthcare Information; 1987. p. 153–64.
9. Kuikka JT, Bergstrom KA, Ahonen A, Lansimies E. The dosimetry of iodine-123 labelled 2 beta-carboxymethoxy-3 beta (4-iodophenyl)tropane. Eur J Nucl Med. 1994;21:53–6.
10. Laruelle M, Wallace E, Seibyl JP, Baldwin RM, Zea Ponce Y, Zoghbi SS, et al. Graphical, kinetic, and equilibrium analyses of in vivo [123I] beta- CIT binding to dopamine transporters in healthy human subjects. J Cereb Blood Flow Metab. 1994;14:982–94.
11. De Keyser, DeBacker JP, Ebinger G, Vauquelin G. Hydrogen-3-GBR-12935 binding to dopamine uptake sites in the human brain. J Neurochem. 1989;53:1400–4.
12. Innis RB, Cunningham VJ, Delforge J, Fujita M, Gjedde A, Gunn RN, et al. Consensus nomenclature for in vivo imaging of reversibly binding radioligands. J Cereb Blood Flow Metab. 2007;9:1533–9.
13. Rorden C, Brett M. Stereotaxic display of brain lesions. Behav Neurol. 2000;12:191–200.
14. Rakshi JS, Uema T, Ito K, Bailey DL, Morrish PK, Ashburner J, et al. Frontal, midbrain and striatal dopaminergic function in early and advanced Parkinson's disease: a 3D [18F]dopa-PET study. Brain. 1999;122:1637–50.
15. Ashburner J, Andersson JL, Friston KJ. Image registration using a symmetric prior – in three dimensions. Hum Brain Mapp. 2000;9:212–25.
16. Shao J. Linear model selection by cross-validation. J Am Stat Assoc. 1993;88:486–94
17. Worsley KJ, Marrett S, Neelin P, Vandal AC, Friston KJ, Evans AC. A unified statistical approach or determining significant signals in images of cerebral activation. Hum Brain Mapp. 1996;4:58–73.
18. le Cessie S, van Houwelingen JC. Ridge estimators in logistic regression. Appl Stat. 1992;41(1):191–201.
19. Hoerl AE, Kennard RW. Ridge regression: biased estimation for nonorthogonal problems. Technometrics. 1970;12:55–67.
20. Hall M, Eibe F, Holmes G, Pfahringer B, Reutemann R, Witten IH. The WEKA data mining software: an update. SIGKDD Explorations. 2009;11:1.
21. Seppi K, Scherfler C, Donnemiller E, Virgolini I, Schocke M, Goebel G, et al. Topography of dopamine transporter availability in PSP: voxel wise analysis of [123I]β-CIT SPECT. Arch Neurol. 2006;63:1154–60.
22. Brucke T, Asenbaum S, Pirker W, Djamshidian S, Wenger S, Wober C, et al. Measurement of the dopaminergic degeneration in Parkinson's disease with [123I] beta-CIT and SPECT. Correlation with clinical findings and comparison with multiple system atrophy and progressive supranuclear palsy. J Neural Transm Suppl. 1997;50:9–24.
23. Kim YJ, Ichise M, Ballinger JR, Vines D, Erami SS, Tatschida T, et al. Combination of dopamine transporter and D2 receptor SPECT in the diagnostic evaluation of PD, MSA, and PSP. Mov Disord. 2002;17(2):303–12.
24. Brooks DJ, Salmon EP, Mathias CJ, Quinn N, Leenders KL, Bannister R, et al. The relationship between locomotor disability, autonomic dysfunction, and the integrity of the striatal dopaminergic system in patients with multiple system atrophy, pure autonomic failure, and Parkinson's disease, studied with PET. Brain. 1990;113:1539–52.
25. Wenning GK, Tison F, Ben-Shlomo Y, Daniel SE, Quinn NP. Multiple system atrophy: a review of 203 pathologically proven cases. Mov Disord. 1997;12:133–47.
26. Papp MI, Lantos PL. The distribution of oligodendroglial inclusions in multiple system atrophy and its relevance to clinical symptomatology. Brain. 1994;117:235–43.
27. Revesz T, Sangha H, Daniel SE. The nucleus raphe interpositus in the Steele-Richardson-Olszewski syndrome (progressive supranuclear palsy). Brain. 1996;119:1137–43.
28. Pascual J, Figols J, Grijalba B, Gonzalez AM, del Olmo E, Berciano J, et al. Changes in aminergic receptors in a PSP postmortem brain: correlation with pathological findings. J Neural Transm Suppl. 1994;42:247–60.
29. Dickson D. Neuropathology of parkinsonian disorders. In: Jankovic J, Tolosa E, editors. Parkinson's disease and movement disorders. Philadelphia: Lippincott Williams and Wilkins; 2002. p. 256–69.
30. Litvan I, Hauw JJ, Bartko JJ, Lantos PL, Daniel SE, Horoupia DS, et al. Validity and reliability of the preliminary NINDS neuropathologic criteria for progressive supranuclear palsy and related disorders. J Neuropathol Exp Neurol. 1996;55:97–105.
31. Osaki Y, Wenning GK, Daniel SE, Hughes A, Lees AJ, Mathias CJ, et al. Do published criteria improve clinical diagnostic accuracy in multiple system atrophy? Neurology. 2002;59:1486–91.
32. Osaki Y, Ben Shlomo Y, Lees AJ, Daniel SE, Colosimo C, Wenning G, et al. Accuracy of clinical diagnosis of progressive supranuclear palsy. Mov Disord. 2004;19:181–9.
33. Hoffman EJ, Huang SC, Phelps ME. Quantitation in positron emission computed tomography: 1. Effect of object size. J Comput Assist Tomogr. 1979;3:299–308.
34. Kojima A, Matsumoto M, Takahashi M, Hirota Y, Yoshida H. Effect of spatial resolution on SPECT quantification values. J Nucl Med. 1989;30:508–14.
35. Mazziotta JC, Phelps ME, Plummer D, Kuhl DE. Quantitation in positron emission computed tomography: 5. Physical-anatomical effects. J Comput Assist Tomogr. 1981;5:734–43.